Positive and Negative Retinotopic Codes in the Human Hippocampus

Peter A. Angeli[1,5*†], Adam Steel[2,3†], Caroline E. Robertson[1,4**]

[1] Department of Psychology, Dartmouth College, Hanover, NH, USA

[2] Beckman Institute, University of Illinois Urbana-Champaign, Urbana, IL, USA

[3] Department of Psychology, University of Illinois Urbana-Champaign, Urbana, IL, USA

[4] Senior Author

[5] Lead Contact

* Correspondence: peter.a.angeli@dartmouth.edu

** Correspondence: caroline.e.robertson@dartmouth.edu

† These authors contributed equally to this work

Competing interest: The authors declare no competing interests.

Data availability: All raw and minimally processed data is made publicly available via the Natural Scenes Dataset (naturalscenesdataset.org). All code required to reproduce the results in this manuscript will be made available in the Open Science Framework repository upon publication.

Acknowledgements: The authors would like to thank the Natural Scene Dataset authors for making their data publicly available. This work was supported by funding from the National Institutes of Mental Health under award number R01MH130529 to CER.

Author contributions: P.A.A., A.S., and C.E.R designed the study, analyzed the data, and interpreted the experiments; P.A.A. and C.E.R. wrote and edited the manuscript; A.S. edited the manuscript. C.E.R. secured funding.

Number of Figures: 5

Number of Tables: 0

Number of Supplemental Figures: 1

Abstract Word Count: 205

Main Text + Figure Legend Word Count: 7261

Abstract

The hippocampus sits at the apex of the visual hierarchy, yet little is known about the visual properties of this core memory structure. Recent work suggests that a latent, bivalent retinotopic code persists in large-scale memory networks at the cortical apex, scaffolding interactions with sensory networks. Here, we tested whether a bivalent retinotopic code also persists within the hippocampus. To do this, we leveraged densely-sampled high-resolution 7T functional MRI along with voxel-scale visual population receptive field (pRF) modeling. Our findings reveal a robust, voxel-scale retinotopic code broadly distributed across subfields and along the long axis of the human hippocampus, comprised of roughly equal proportions of pRFs with positive and negative amplitude responses to visual stimulation. Hippocampal pRFs displayed canonical visual properties, including stable valence and visual field preferences across runs and a contralateral bias. Retinotopic structure also persisted at rest: hippocampal voxels with similar pRF locations were more strongly correlated than voxels representing different visual field locations. Finally, across the ventral visual stream, the prevalence of negative-amplitude pRFs increased with mnemonic involvement, culminating in the balanced, bivalent organization within the hippocampus. These findings support the view that sensory and mnemonic systems are coupled through a shared retinotopic code at the apex of the visual hierarchy.

Introduction

The hippocampus serves as a critical hub for sensory-mnemonic interactions, integrating sensory information with memory processing to support the encoding and retrieval of episodic memories (Scoville and Milner 1957; Cohen and Squire 1980; Cohen and Eichenbaum 1993). As such, hippocampal representations essentially rely on input from sensory systems, including the visual system (Vinogradova 2001; Jeffery 2007; Pereira et al. 2007). Yet relatively little is known about the visual coding properties of this core memory structure.

Classic models of cortical organization place the hippocampus at the apex of the visual hierarchy (Felleman and Van Essen 1991), where it is thought to construct abstract, internal models of the external world. Canonically, hippocampal coding schemes are thought to be primarily allocentric and context-dependent (Scoville and Milner 1957; O'Keefe and Dostrovsky 1971; Cohen and Squire 1980; Cohen and Eichenbaum 1993; Eichenbaum and Cohen 2014; Whittington et al. 2020), fundamentally distinct from sensory-driven retinotopic codes like those found in early visual areas (Sereno and Allman 1991; Tootell et al. 1998). However, recent findings challenge this view. Work in rodents and nonhuman primates has shown that a significant proportion of hippocampal neurons exhibit egocentric visual coding (Acharya et al. 2016; Gulli et al. 2020; Purandare et al. 2022), and human fMRI research has identified visual field preferences in hippocampal voxels (Knapen 2021; Silson et al. 2021). Thus, contrary to the classic view, these cross-species findings suggest the hippocampus may demonstrate egocentric visual coding, but evidence from cerebral cortex indicates these descriptions may be incomplete.

Recent studies of retinotopic coding in memory-related cortical regions, like the Default Network (DN), have observed atypical retinotopic coding alongside classic mnemonic responses. Specifically, many of the DN's retinotopic responses exhibit a negative valence — that is, decreasing activity in response to visual presentation (Szinte and Knapen 2020; Klink et al. 2021; Knapen 2021; Steel et al. 2024b) — in contrast to the typical positive valence found in visual areas. This bivalent (positive and negative) retinotopic code structures a voxel-scale push-pull dynamic between perceptual and mnemonic cortical regions and networks (Steel et al. 2024b, 2024a). One hypothesis is that a similar bivalent retinotopic code might exist in the hippocampus, given the structure's well-characterized mnemonic properties and connectivity with the DN (Greicius et al. 2004; Vincent et al. 2006; Kahn et al. 2008).

In this study, we used high-resolution 7T functional MRI from visual mapping tasks to test whether a bivalent retinotopic code is present within the human hippocampus. In brief, our results show that the human hippocampus contains a robust retinotopic code, with a balanced proportion of positive and negative population receptive fields (pRFs), evenly distributed throughout the hippocampus. Importantly, this code is reliable: pRF amplitude and valence are consistent across runs of the retinotopic mapping task. Both positive and negative pRFs demonstrate a bias towards the contralateral visual field, and we found the proportion of negative pRFs increases moving up the ventral visual stream hierarchy, parallelling mnemonic involvement. Finally, during resting-state fixation, retinotopic preferences strongly influence the correlation of activity among hippocampal pRFs, suggesting that this bivalent retinotopic code may be broadly relevant for mnemonic information processing in the hippocampus.

Methods

Overview

We used data made publicly available through the Natural Scenes Dataset (NSD, Allen et al. 2022) that included 8 participants scanned extensively at 7T over the course of several days. The high resolution of the data allowed for detailed explorations of hippocampal activity. Relevant to the present study, each participant completed *both* three runs of sweeping bar retinotopic mapping task and at least 14 runs of a resting-state fixation task (range: 14 – 34 runs). Retinotopy and fixation data were minimally preprocessed using manual ICA denoising, and all subsequent analyses were performed in participant-specific volume space. To allow for the identification of negative retinotopic responses, population receptive field (pRF) modeling was performed using AFNI's mapping procedure (3dNLfim). We did not regress global signal, and data were left unsmoothed.

Data Preparation

Participants and Data Acquisition

Data from the eight participants (ages 19 – 32) included in the NSD release were used for the current study. One participant (subj03) was excluded from all analyses due to an insufficient quantity of resting-state fixation data that passed our quality control criteria (see Quality Control and Preprocessing below). The final set of seven participants had a mean age of 26.1 yr (7 right-handed; 5 women) and had normal or corrected-to-normal visual acuity. All participants provided informed consent for the study.

MRI data was acquired at the Center for Magnetic Resonance Research at the University of Minnesota as described in Allen et al. (2022), and the study was approved by the University of Minnesota institutional review board. Briefly, anatomical scans were acquired using a 3T Siemens Prisma scanner with a 32-channel head coil, including several T_1-weighted magnetization prepared rapid acquisition gradient echo (MPRAGE, voxel size = 0.8 mm^3 isotropic, TR = 2,400 ms, TE = 2.22 ms, flip angle = 8°, in-plane acceleration factor = 2) and T_2-weighted sampling perfection with application-optimized contrasts using different flip angle evolution sequence (SPACE, voxel size = 0.8 mm^3 isotropic, TR = 3,200 ms, TE = 563 ms, in-plane acceleration factor = 2) acquisitions. The remaining data was acquired on a 7T Siemens Magnatom scanner and a single-channel-transmit, 32-channel-receive head coil. Functional data were gradient-echo echo-planar scans (voxel size = 1.8 mm^3 isotropic, TR = 1,600 ms, TE = 22 ms, flip angle = 62°, matrix = 120 x 120, field-of-view = 216 mm x 216 mm), corrected with dual-echo fieldmaps (matched slice prescription to EPI, voxel size = 2.2 mm x 2.2 mm x 3.6 mm TR = 510 ms, TE = 8.16 ms, TE = 9.18 ms). For improved hippocampal segmentation, an additional T_2-weighted turbo-spin echo scan was collected (voxel size = 0.357 mm x 0.357 mm x 1.5 mm, 56 oblique slices perpendicular to anterior-posterior axis of the hippocampus, TR = 16,000 ms, TE = 53 ms, in-plane acceleration factor = 2).

Task Paradigms

The retinotopic mapping paradigm (adapted from the Human Connectome Project Retinotopy Dataset; Benson et al. 2018, RETBAR1 and RETBAR2) consisted of a bar aperture slowly moving across the visual field, revealing objects at multiple scales (i.e. faces, houses, and objects) superimposed on a pink-noise background (Fig. 1A). Both the apertures and textures updated at a rate of 15 Hz, and covered a circular region with a diameter of 8.4°. For each 300 second run, participants were instructed to fixate on a small (0.2° x 0.2°) semi-transparent dot in the center of the screen, and indicate with a button press whenever the color of the dot changed (which occurred every 1 – 5 sec). Three runs of this task were collected, for a total of 15 minutes of data. Additional wedge/ring runs were also acquired as part of the NSD, but consistent with other studies characterizing −pRFs (Szinte and Knapen 2020; Klink et al. 2021; Steel et al. 2024b) here we consider only the bar stimulus,.

In all resting-state fixation tasks, participants were instructed to fixate on a small white cross (0.5° x 0.5°) in the center of a gray screen. In each session where fixation tasks were acquired, one run was collected at the beginning of the session, and the other at the end. The first fixation run included no additional instructions. For the second fixation run, participants were instructed to take a deep breath 12 sec after the beginning of the run, when the fixation cross turned red

for 4 sec. Each run of fixation was 300 sec, and between 14 and 34 runs (70-170 minutes of data) were collected for each participant.

Quality Control and Preprocessing

All data was assessed for quality prior to inclusion in the dataset as described in the original data release (Allen et al. 2022). Motivated by the sensitivity of resting-state functional connectivity to data quality, particularly motion, we performed additional quality control measures on the fixation data. We assessed the quality of resting-state fixation data using AFNI's quality control report creation tool (APQC, Taylor et al. 2024), and excluded any fixation run with a maximum displacement of greater than 1.8 mm, or a framewise displacement greater than 0.12 mm. Runs with a maximum displacement between 1 mm and 1.8 mm, and a framewise displacement of between 0.1 mm and 0.12 mm, were assessed on a case-by-case basis, and excluded if the movement was the result of large shifts (approach similar to Du et al. 2024). For functional connectivity analyses we removed the first 25 TRs (40s) of every fixation run, leaving 260 sec (4.25 min) of data, to remove artifacts associated with the instructed deep breath during the second fixation run in each session. After these exclusions, one participant (subj03) had only a single fixation run remaining (4.25 min), and so was excluded from the present study's analyses. The other 7 participants had between 8 and 24 runs (mean: 14, sd: 6.13, 34 – 102 min) of high-quality fixation data.

Retinotopy and fixation data were minimally preprocessed, including unwarping and aligning, as described in the NSD data release (Allen et al. 2022). We further denoised the data via manual ICA classification (Griffanti et al. 2014, 2017; Steel et al. 2021b), as automated ICA denoising tools have poor performance on high resolution data like the NSD (Beckers et al. 2023). For each run, the time series was decomposed into independent spatial components along with their associated temporal signal using FSL's melodic ICA (Beckmann and Smith 2004). We then assigned each component to either signal or noise using established criteria (Griffanti et al. 2017). After classification, all the noise components were regressed from the data (fsl_regfit; Griffanti et al. 2014), and the resulting denoised time course was normalized to percent signal change. We did not perform global signal regression (Saad et al. 2012), and all functional data was left unsmoothed.

Retinotopic Mapping

Population Receptive Field Modeling

To perform population receptive field (pRF) modeling, we average all three denoised and normalized retinotopy runs together to produce an average retinotopy time series, to which we applied the AFNI modeling procedure using 3dNLfim as described in Silson et al. (2015). The model calculated 4 million possible 2D Gaussian receptive fields with a given center position and size based on the timing of the presented sweeping bar (resampled to the temporal resolution of the fMRI acquisition, TR = 1.333s). For each voxel, the best of these predicted time series was chosen after the application of a flexible amplitude scalar, using a combination of

Simplex and Powell optimization algorithms, minimizing the least-squares error between the acquired BOLD time series and the amplitude-scaled prediction. Importantly, amplitude here reflects the relative activation/deactivation of a given voxel to visual stimulation of its receptive field. Group data was generated for visualization only by averaging the amplitude estimate across participants for all vertices on the AFNI standard 141 surface, without screening for significance (see Reliability and Stability of Hippocampal pRF Modeling below).

Reliability and Stability of Hippocampal pRF Modeling

To establish the reliability of our pRF model in the hippocampus, we compared task-derived model fits to those of a control null distribution for each participant. To generate this control null distribution of model fits, we applied the retinotopic model to hippocampal activity during a task that would not be expected to have systematic retinotopic visual field stimulation: resting-state fixation. For each participant, we first averaged the time course of all resting-state fixation runs prior to trimming, which were matched in length to the retinotopy task runs (300s). Then, we applied the retinotopic model to the average hippocampal resting state activity to derive model fits for each hippocampal voxel. Critically, because participants did not see the sweeping bar stimulus during resting-state fixation, this produces a null distribution of model parameters. We used this null distribution to determine an empirically-derived noise floor within the hippocampus. This was important because previous pRF research has applied R^2 cutoffs based on data in visual areas, and it is not a given that the hippocampus would have a comparable noise-floor to visual areas. We chose a noise floor corresponding to the 95th percentile R^2 value of the null model (0.117), and only considered voxels with fits that exceeded this floor to be retinotopic.

In addition to requiring fits above the noise floor, we conservatively screened voxels based on model estimates of size (sigma) and eccentricity, guided by the size of the presented stimulus (diameter 8.4°, bar width 1.05°). Specifically, we excluded any voxels with a size estimate smaller than .42° or larger than 3.78° (10% and 90% of the largest possible sigma estimate), as well as voxels with an eccentricity estimate greater than 3.78° (90% of maximum possible eccentricity). Voxels that passed the above noise floor, size, and eccentricity screens were determined to be “significant pRFs”, while all others were “non-significant voxels.”

Finally, we sought to validate the stability of retinotopic features (amplitude sign and center position) between individual runs of the sweeping bar retinotopy task. To do so, we fit the above pRF model on each individual run of the sweeping bar stimulus, rather than the average, producing three sets of model parameters for each hippocampal voxel. To ensure that voxel categorization would not differ across runs, we used model parameters derived from the three-run average to determine significance (based on model fit, size, and eccentricity as described above). To assess center position stability, we calculated the average Euclidean distance for each significant voxel between all three pairings of sweeping bar runs (i.e. run 1 – run 2, run 1 – run 3, and run 2 – run 3). We quantified amplitude sign stability by binarizing voxels according to their amplitude, and calculated a 3-run Dice coefficient ($coefficient = \frac{3|run1 \cap run2 \cap run3|}{|run1|+|run2|+|run3|}$). We applied this separately to positive amplitude voxels (i.e. significant pRFs with positive amplitudes binarized to 1, other significant pRFs set to 0) and negative amplitude voxels

(significant pRFS with negative amplitudes binarized to 1, other significant pRFs set to 0), resulting in two, amplitude-specific, coefficients per participant. The significance of these stability measures was established on a participant-level by z-scoring the values described above (derived from significant voxels) against 5000 additional measures derived from a random sampling of all hippocampal voxels, both significant and non-significant, matched in number to the number of significant pRFs.

ROI creation

To contextualize hippocampal pRFs within the ventral visual stream, we extracted cortical pRF data within three group-level ROIs: early visual cortex, the parahippocampal place area (PPA), and the ventral place memory area (vPMA). Early visual cortex was first defined on the participant-level to include V1, V2, and V3, as identified in the NSD release via retinotopic features (Allen et al. 2022). We then projected these participant specific ROIs to the standard 141 surface, and quantified the overlap across participants. Finally, the group ROI was constrained to vertices that fell within the early visual ROI in 4 or more participants. Group-level ROIs for PPA and vPMA were derived from publicly available dataset of probabilistic ROIs on the standard 141 surface (Steel et al. 2025), identified via scene perception tasks for PPA and scene memory tasks for vPMA. We included vertices with a probability of >20%, and further constrained the ROIs to be non-overlapping. This was achieved by visually identifying the anterior-posterior midpoint of the overlapping region, and defining PPA as posterior to that point, and vPMA as anterior. For consistency with the hippocampal analyses, pRF data was extracted in the volume by projecting each group ROI from the standard 141 surface into each participant's volume-space.

Within the hippocampus, we defined ROIs for hippocampal subfields and relative position along the long (anterior-posterior) axis of the hippocampus. Participant-specific subfield ROIs, included in the NSD release, were calculated using the Freesurfer automated segmentation and visually inspected prior to use. To explore differences along the hippocampal long axis, each participant's hippocampus was divided into 18 segments equally spaced along the y dimension of volume space.

Visual Field Coverage

To assess the visual field coverage of hippocampal pRFs, we applied a max-operator approach similar to Silson et al. (2021) and Steel et al. (2024b). In each participant, we reconstructed the 2D Gaussian corresponding to each significant pRF, with the amplitude scaled by that voxel's model fit (R^2). We refer to values derived from this Gaussian as pRF values. Next, for each participant we calculated the maximum pRF value at each point in the visual field across all significant pRFs with a given amplitude (positive or negative) and subsequently performed participant-specific normalization of pRF values such that the maximum value would be 1. These maximum-operator maps were then averaged to generate the group-level coverage maps. To calculate visual field bias, in each participant the X coordinate of peak maximum-value from the left hemisphere was averaged with the right hemisphere's peak value X coordinate multiplied by −1. Statistical significance was assessed using a one-sided t-test with the

alternative hypothesis that the mean visual field bias is greater than 0, indicating a contralateral bias.

Functional Connectivity Analyses

Influence of Retinotopic Valence

We used a resting-state functional connectivity approach to explore how pRF model valence predicts intrahippocampal interactions. First, we averaged the time courses of hippocampal +pRFs, −pRFs, and non-significant voxels for each run of resting-state fixation. No spatial smoothing was applied to resting-state runs to preserve voxel-level differences, and keep preprocessing consistent with retinotopic mapping runs. We calculated the run-level partial correlation between the average + and −pRF time courses in each participant, controlling for global hippocampal correlation via the average non-significant voxel's time course, then Fisher z-transformed the resulting correlations. Statistical significance was calculated at the participant-level via paired and one-sided t-tests.

Influence of Retinotopic Alignment

To better understand the influence of retinotopic features beyond valence on functional connectivity, we investigated differences in functional connectivity between pairs of pRFs sensitive to either similar or different portions of the visual field, which we term retinotopic alignment. To assess the influence of retinotopic alignment within the hippocampus, we took each hippocampal pRF sequentially as a source and sorted hippocampal pRFs within the same hemisphere of the same or opposite valence according to the Euclidian distance between that pRF's center and the source pRF center. We defined the pRF with the smallest difference in Euclidian distance to be retinotopically aligned ("Matched"), and randomly sampled 1 voxel from the 1/3 of voxels with the largest distance 1000 times to generate a group of non-aligned voxels ("Random"). We then calculated the run-level partial correlation between the source voxel, the matched voxel, and each of the random voxels, controlling for the average activity of non-significant hippocampal voxels. Finally, these values were Fisher z-transformed, averaged across runs, and the random voxels further averaged to generate a single correlation value. After completing this process for every source voxel, we averaged the matched and random correlation values according to the valence of the source and target pRFs to generate 4 participant-level estimates for retinotopic alignment: 1) matched, same valence 2) matched, opposite valence 3) random, same valence 4) random, opposite valence.

Statistical Tests

All statistical analyses were performed using R (version 4.3.2). Specific tests are described in the relevant portions of the Results and Methods. In summary: run-level significance for retinotopic modeling R^2 was assessed using Kolmogorov-Smirnov test while other feature reliability measures (center position, valence) were z-scored relative to estimates sampled from

all hippocampal voxels. We used a linear mixed effects model to assess the contribution of brain region to the proportion of −pRFs, controlling for mean R^2. All other analyses were assessed using t-tests.

Results

We first determined the presence of retinotopic coding in the human hippocampus. To do this, we performed voxel-scale population receptive field (pRF) modeling (Dumoulin and Wandell 2008, for implementation see Cox 1996, 2012) on high-resolution 7T fMRI data from the hippocampus during a visual retinotopic mapping task (Fig. 1A).

To validate the reliability of the task-driven retinotopic response in the hippocampus, we compared task-derived model fits to a control null distribution (Fig. 1B), which was generated by applying the retinotopic model to hippocampal activity during independent runs of resting-state fixation data from the same participants (see Methods). Task-derived model fits were significantly better than the null model fits (within participants: paired t-test, $t(6) = 3.779$, $p < 0.01$; across participants: asymptotic two-sample Kolmogorov-Smirnov Test, H_a: task < null, $D^- = 0.224$, $p < 0.001$). To ensure that the hippocampal null distribution did not reflect an elevated baseline susceptibility to model noise relative to classic retinotopic regions, we compared resting-state null fits in the hippocampus to those in early visual cortex (EVC). Null R^2 values were comparable across the regions (EVC $R^2 = 0.062$ +/− 0.005; Hippocampus $R^2 = 0.060$ +/− 0.002) (Supplemental Fig. 1), indicating that the hippocampus is not uniquely susceptible to spurious retinotopic fits. We therefore defined a voxel as retinotopic if its pRF model fit exceeded the hippocampal noise floor, defined as the 95th percentile of the null distribution ($R^2 = 0.117$, Fig. 1B, see Methods). Voxels meeting these criteria were classified as retinotopic and are referred to throughout the manuscript as “pRFs” or “significant voxels”.

We observed pRFs throughout the hippocampus (Fig. 3A), with an approximately equal mix of positive and negative valences (+/− pRFs). We did not observe a significant hemispheric difference in the proportion or absolute number of significant voxels (proportion: $t(6) = .275$, $p = .792$; abs. number: $t(6) = .190$, $p = 0.855$), and so pooled analyses across both hemispheres. On average across all participants, approximately 9% (8.6%, +/− 1.88%) of hippocampal voxels were significantly retinotopic, with approximately half (54.7%, +/− 6.99%) of the significant voxels showing a negative valence (−pRFs). Negative pRFs, like positive pRFs, showed robust stimulus-evoked responses, characterized by stimulus-locked suppression of activity rather than increased activation (Fig. 1A, right). Importantly, positive and negative pRFs exhibited comparable model fits (Fig. 1C; −pRF mean $R^2 = 0.167$ +/− 0.006, +pRF mean $R^2 = 0.166$ +/− 0.006; within participants: $t(6) = 0.106$, $p = 0.918$; across participants: $D = 0.10$, $p = 0.11$), indicating that our modeling approach does not preferentially bias fits toward positive response amplitudes. Together, these findings indicate that hippocampal retinotopy is supported by both positive and negative response profiles that are equally robust and equally well captured by the pRF model.

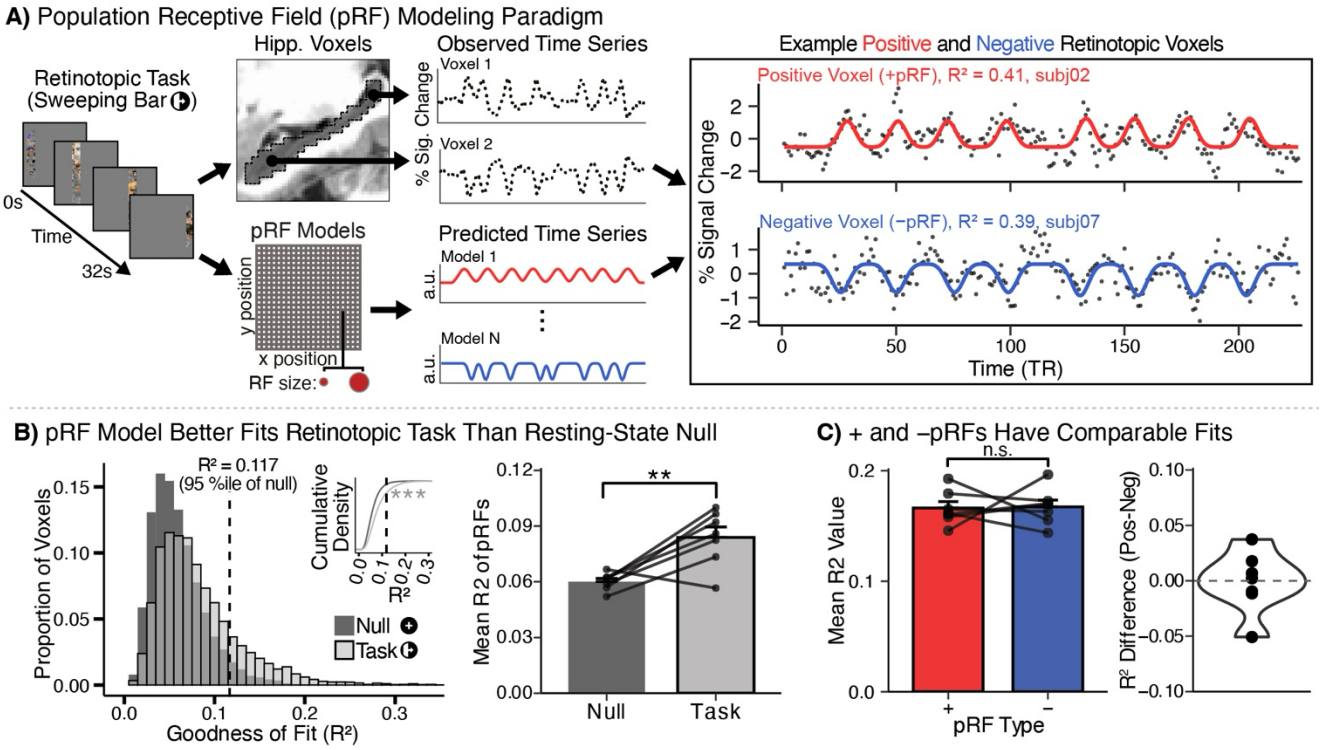

Fig. 1. Reliable positive and negative population receptive fields (pRF) in the human hippocampus. A. Schematic of fMRI population receptive field (pRF) modeling procedure. *Voxel time series from a sweeping bar visual mapping task (Benson et al. 2018; Allen et al. 2022) were fit with a 2D Gaussian pRF model varying in center location (x,y), size (degrees visual angle), and amplitude (positive or negative). Voxels with a positive amplitude parameter are termed +pRFs, while those with negative amplitude parameters are termed −pRFs. Schematic of theoretical time courses (points) with model prediction (line) highlight the impact of amplitude. Example time courses (right) illustrate stimulus-evoked activation for +pRFs and suppression for −pRFs relative to baseline.* ***B. Task-derived pRF model fits in the hippocampus exceeded those obtained from a null distribution generated using resting-state fixation data****. Across hippocampal voxels (pooled across n=7 participants), task-derived model fits were significantly right-shifted relative to null fits.* ***C. Positive and negative pRFs had similar goodness-of-fit (R^2) values after thresholding.*** *(Left) Subject-level mean R^2 for +pRFs (red) and −pRFs (blue). There was no significant difference between valences. (Right) Subject-level difference in mean R^2 between +pRFs and −pRFs (no significant difference). ***p < 0.001 **p < 0.01 *p < 0.05*

As an additional validation, we assessed whether the retinotopic features of hippocampal pRFs were stable between identical runs of the visual mapping task. Hippocampal pRFs showed strong reliability across identical runs (Fig. 2A). Across pRF voxels, both center position estimates (i.e., preferred visual field location) and response valence (i.e., positive vs. negative

responses) were highly reliable across different runs of the sweeping bar task, significantly outperforming a reference distribution of voxels generated by sampling from all hippocampal voxels (see Methods; 6/7 center position *p*-values < 0.01; all valence *p*-values < 0.05). Thus, hippocampal pRFs demonstrated run-level stability in both a core retinotopic property — preferred visual field location — and the more novel dimension of response valence.

Motivated by prior reports of a contralateral visual field bias in positive hippocampal pRFs (Knapen 2021; Silson et al. 2021), we tested whether both valences of the observed bivalent code have the same bias. At the group level, both +pRFs and −pRFs trended towards contralateral visual field biases (see Methods; +pRF mean bias: 0.27 +/− 0.05; −pRF mean bias: 0.11 +/− 0.08; Fig. 2B). This bias was significant for the +pRF subpopulation alone ($t(6) = 5.230$, $p < 0.001$), and did not reach significance for −pRFs ($t(6) = 1.394$, $p = 0.11$). Nevertheless, most participants (5/7) showed a numerical contralateral bias, as evident in group-level plots (Fig. 2B, right).

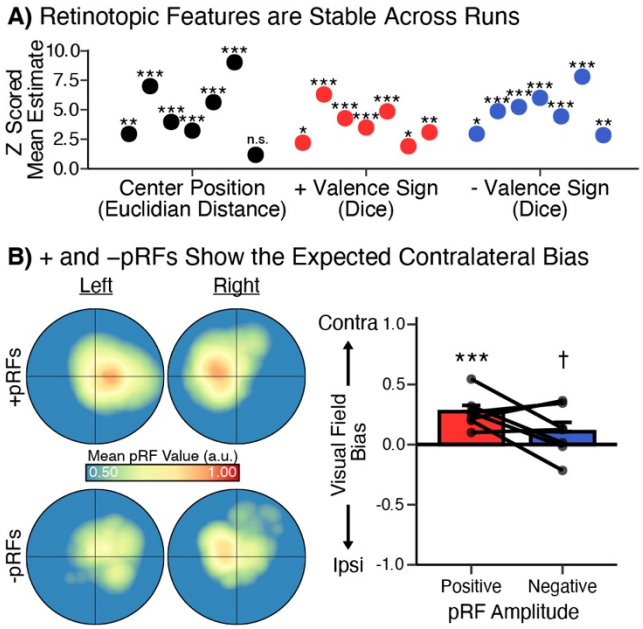

Fig. 2. Hippocampal pRFs are stable across runs and exhibit contralateral bias. A. Run-to-run stability of retinotopic features. *Center position (black) and valence (+, red; −, blue) were consistent across individual runs of the retinotopic mapping task. Center position consistency was calculated using average Euclidian distance between pairs of runs (black dots), while valence sign was calculated using a 3-run Dice coefficient (red and blue dots). Coefficients derived from voxels with significant pRF fits were z-scored relative to all hippocampal voxels. Each point is a participant, from left to right: subj01, subj02, subj04, subj05, subj06, subj07, and subj08.* ***B. Contralateral bias of + and − pRFs.*** *(Left) Mean visual field coverage using a max-operator (see Methods) (Right) Participant-level maximal bias shows that hippocampal +pRFs preferentially cover the contralateral visual field ((0.27 ± 0.05; one-sided t-test, $t(6) = 5.23$, $p < 0.001$)). −pRFs showed a trend for the contralateral hemifield (0.11 ± 0.08; $t(6) = 1.39$, $p = 0.106$). ***p < 0.001 **p < 0.01 *p < 0.05*

Extensive evidence suggests functional and organizational differentiation along the hippocampal long axis and subfields (for review see Poppenk et al. 2013; Strange et al. 2014); therefore, we next explored the relative concentration of +/− pRFs along the hippocampal long axis. We found a uniform spatial distribution of retinotopic voxels within the hippocampus (Fig. 3), with no significant difference in the prevalence of +/− pRFs along the long axis (Fig. 3B; $F(1, 118) = 0.608$, $p = 0.437$) or between subfields (Fig. 3C; $F(8, 48) = 1.268$, $p = 0.283$). This even distribution held when considering only +pRFs (long axis: $F(1, 118) = 0.916$, $p = 0.341$; subfields: $F(8, 48) = 1.284$, $p = 0.274$) or −pRFs (long axis: $F(1, 118) = 2.53$, $p = 0.115$; subfields: $F(8, 48) = 1.070$, $p = 0.399$).

Despite this overall uniformity, we observed qualitative variability in the absolute prevalence of retinotopic voxels across subfields. The subiculum, CA4, and molecular and granular cell layers of the dentate gyrus showed the lowest overall proportion of retinotopic voxels (subiculum: 5.9% +/− 1.6%; CA4: 6.4% +/− 2.3%; DG Mol. and Gran.: 7.0% +/− 2.0%). Interpretation of the relative proportions of positive and negative pRFs within individual subfields is limited by the fact that some participants lacked significant pRFs in certain subregions, resulting in an uneven number of observations across subfields (n = 5 – 7). With this caveat, the parasubiculum has the highest prevalence of −pRFs (proportion of all pRFs: 70.0% +/− 18.6%, n = 5; proportion of all voxels: 8.4% +/− 4.2%, n = 7) while CA4 has the highest proportion of +pRFs (proportion of all pRFs: 59.1% +/− 15.7%, n = 5; proportion of all voxels: 3.0% +/− 1.0%, n = 7). Taken together, the broadly consistent prevalence of positive and negative pRFs across the hippocampus suggests that voxel-scale bivalent retinotopic organization is not restricted to a specific hippocampal subregion, while leaving open the possibility of finer-grained differences within subfields.

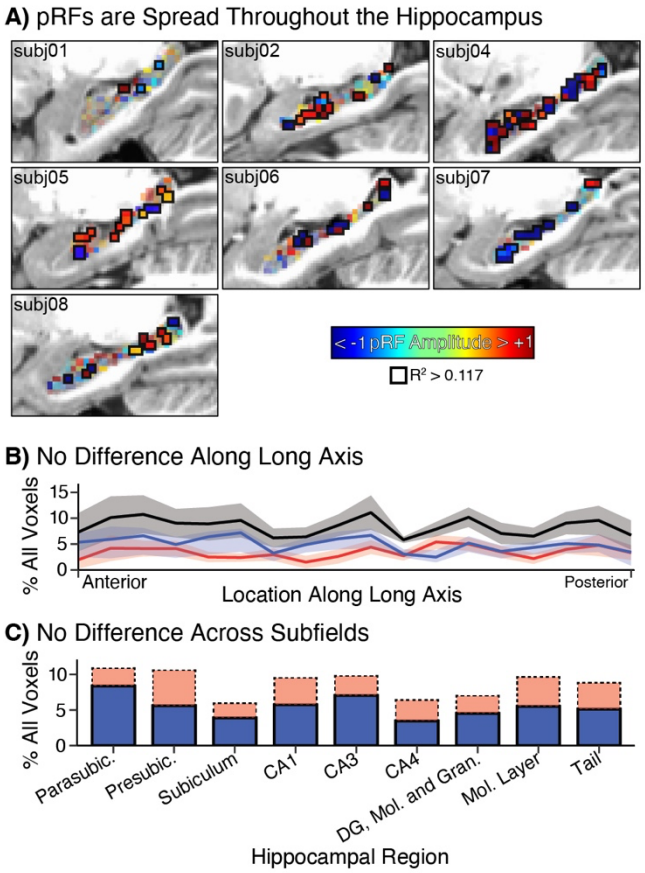

Fig. 3. Retinotopic voxels are evenly distributed within the hippocampus*. *A. Every participant displayed both positive and negative hippocampal pRFs. *Across participants, 9% of hippocampal voxels displayed significant pRFs. Voxel opacity reflects magnitude of R^2 value, and voxels passing significance threshold of 0.117 are outlined.* ***B. No difference in pRF distribution along the long axis.*** *The proportion of significant pRFs (black line) and the proportion of each pRF amplitude (positive: red, negative: blue) calculated in 18 bins along the hippocampal long axis. Neither the proportion of significant pRFs (black line) nor the proportion of +/− pRFs (red and blue lines, respectively) significantly differed along the long axis (p = 0.115 – 437).* ***C. No difference in pRF distribution between subfields.*** *Despite qualitative differences in some subfields, notably the subiculum, we found no statistically significant difference across subfields in the overall proportion of significant pRFs or prevalence of specific valence (p = 0.283 – 0.399).*

To provide functional context for the hippocampal retinotopic code, we explored whether pRF prevalence and valence follows the pattern established by visual regions lower in the hierarchy — where −pRFs become more prevalent towards mnemonic regions at the cortical apex, in line with their putative functional role in mnemonic processing (Steel et al. 2021a, 2023, 2024b) (Fig. 4). In early visual cortex, 63.3% (se: 1.8%) of voxels are retinotopic and only 14.8% (se: 3.1%) of those have a negative valence. Along the ventromedial visual pathway to the hippocampus (Rolls 2025), the proportion of retinotopic voxels decreases while the proportion of negative voxels increases towards a maximum of 54.7% (se: 7.0%) in the hippocampus (Fig. 4).

Parahippocampal cortex is of particular interest because previous work has identified a functional split between the perceptual parahippocampal place area (PPA) and mnemonic ventral place memory area (vPMA), found in the posterior and anterior portions, respectively, of parahippocampal cortex (Steel et al. 2021a, 2023). Mirroring this functional divide, 17.7% of pRFs in the PPA have a negative amplitude (se: 6.3%), while the immediately anterior vPMA has a much higher proportion of −pRFs (28.7% +/− 4.3%). To ensure that the relatively high proportion of negative pRFs in higher-order regions and the hippocampus was not driven by changes in the average model fit across regions (see Supplemental Fig. 1), we fit a linear mixed-effects model predicting −pRF prevalence from region and mean R^2. Only region identity predicted −pRF prevalence (region: $F(3, 18.308) = 9.712$, $p < 0.001$; mean R^2: $F(1, 22.996) = 0.185$, $p = 0.672$).Thus, consistent with previous work in cortex (Szinte and Knapen 2020; Steel et al. 2024b), these results indicate that the proportion of −pRFs increases ascending the perceptual-mnemonic hierarchy, independent of retinotopic model fit, supporting the interpretation that +/− pRFs differentially relate to perceptual and mnemonic processing.

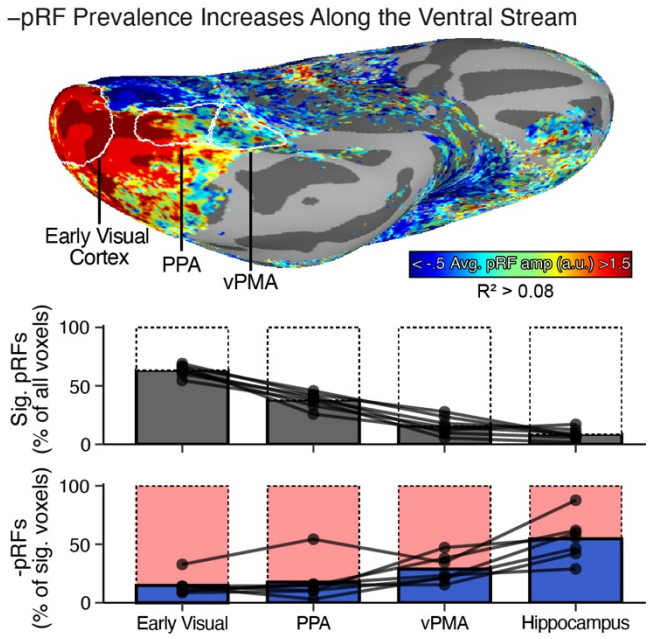

Fig. 4. Negative pRF prevalence increases along the ventral visual stream. (Top) *Cortical ROIs used for ventral stream hierarchy, overlayed on a group-average map of pRF amplitudes. Regions span visual to mnemonic areas along the ventromedial stream: early visual cortex (EVC); parahippocampal place area (PPA); and ventral place memory area (vPMA).* ***(Bottom)*** *Across participants, the overall proportion of significant retinotopic voxels (pRFs) is highest in visual areas and decreases in mnemonic areas. In contrast, −pRF prevalence increases moving up the visual-mnemonic hierarchy, culminating in the hippocampus, with the fewest pRFs and highest proportion of −pRFs.*

In higher order cerebral cortex, including the Default Network (DN), bivalent retinotopic codes structure activity not only during perceptual-mnemonic tasks (Steel et al. 2024b), but also during resting-state fixation (Steel et al. 2024a), suggesting that retinotopy reflects an intrinsic organizational principle of spontaneous activity rather than a task or stimulus-driven effect. A defining feature of this architecture is antagonistic coupling between retinotopically-matched positive and negative pRF populations, thought to structure a push–pull interaction between externally oriented perceptual processing and internally oriented mnemonic processing (Steel et al. 2024b, 2024a). If the hippocampal bivalent code is similarly fundamental, it should continue to shape voxel-scale functional coupling even in the absence of structured visual input. We therefore tested whether the retinotopic properties of hippocampal voxels (valence, visual field location), as estimated during visual mapping, predict voxel-scale activity during independent resting-state fixation runs.

First, we tested whether the functional coupling of hippocampal pRFs during fixation was structured by their valence (i.e., positive vs. negative) (Fig. 5A). Critically, visual stimulation during fixation runs is limited to a small static plus sign in the center of the screen. Despite the absence of structured visual stimulation, activity in opposite-valence pRFs (i.e., positive correlated with negative) was significantly anti-correlated at rest, after controlling for the activity of non-retinotopic voxels ($z(r) = -0.175 +/- 0.065$, $t(6) = 2.696$, $p < 0.05$). Thus, the antagonistic functional relationship identified by bivalent retinotopy is not constrained to visual tasks.

We next asked whether resting-state coupling was structured by retinotopic alignment — that is, whether voxels monitoring similar portions of visual space exhibited stronger functional relationships (Fig. 5B). Pairs of hippocampal pRFs that monitored nearby regions of the visual field (“Matched”) were significantly more anti-correlated than pairs of pRFs that monitored different locations of the visual field (“Random”, $t(6) = 4.707$, $p < 0.01$; see Methods). Conversely, same-valence pRFs with matched receptive fields were more positively correlated than random pairs ($t(6) = 4.274$, $p < 0.01$). Together, these results indicate that retinotopic features predict intrahippocampal functional connectivity at rest, consistent with the view that bivalent retinotopic mapping serves as a general scaffold for structuring spontaneous dynamics within the hippocampus.

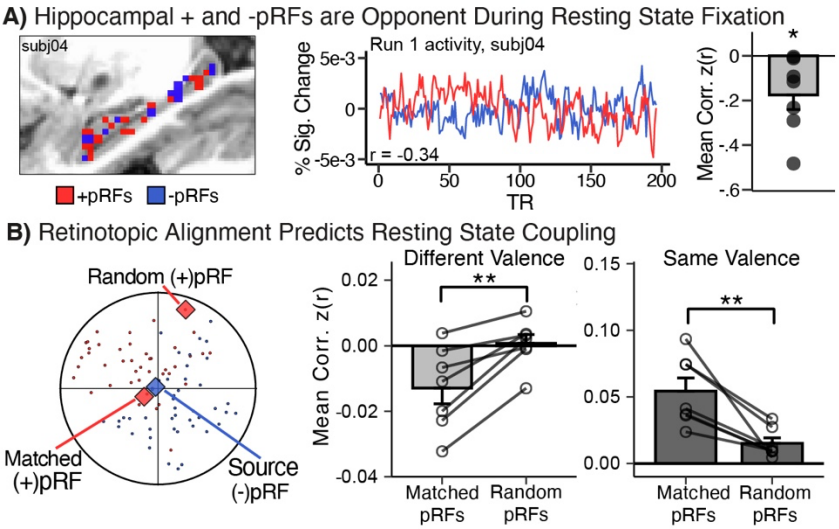

Fig. 5. Retinotopic valence and alignment predict voxel-wise functional coupling within the hippocampus at rest. A. Positive and negative pRFs are anti-correlated at rest (Left) *Example positive and negative hippocampal pRFs.* ***(Middle)*** *Average positive (red) and negative (blue) pRF activity from an example participant during a single run of resting-state fixation, after regressing non-significant voxel activity. Note the broadly anticorrelated activity, despite the lack of dynamic visual stimulation.* ***(Right)*** *Hippocampal +pRFs and −pRFs demonstrate a significant anti-correlation, after controlling for non-significant hippocampal voxels, during task-independent resting-state fixation.* ***B. Retinotopic alignment enhances pRF relationships at rest (Left)*** *Procedure for defining retinotopic alignment. Source pRF activity was correlated with the pRF with the closest visual field location ("Matched"), and this correlation was compared to the mean of a random sampling of pRFs from the furthest 1/3 of pRFs ("Random"). All correlations controlled for the activity of non-significant hippocampal voxels, and were performed for both same-valence (+/+; −/−) and opposite-valence (+/−) pRFs.* ***(Middle and Right)*** *Relative to randomly aligned pRFs, retinotopically aligned hippocampal pRFs of opposite valence were significantly more anti-correlated during fixation, while aligned pRFs of the same valence were significantly more positively correlated. Error bars indicate standard error around the mean. **p < 0.01 *p < 0.05*

Discussion

Here, we identified a bivalent retinotopic code in the human hippocampus, with roughly equal proportions of positive and negative visually-evoked responses (+/−pRFs). These populations exhibit consistent valence and visual field preferences across runs, show a contralateral bias, and are broadly distributed throughout the hippocampus. Critically, this organization is not confined to retinotopic mapping tasks: opposing valence predicts intrinsic anti-correlated coupling at rest, and shared visual field preference strengthens voxel-scale functional connectivity. Together, these findings suggest that retinotopy in the hippocampus reflects an intrinsic organizational principle, rather than simply a consequence of visual stimulation,

potentially serving to link perceptual and mnemonic processing at the apex of the visual hierarchy.

Challenging Conventional Models of the Visual Hierarchy

Our findings challenge conventional views of the brain, which propose that low-level sensory codes like retinotopy are shed as information ascends the visual hierarchy towards the hippocampus (Jeffery 2007; Whitlock et al. 2008; Vann et al. 2009; Clark et al. 2018; Alexander et al. 2023). These models suggest that the hippocampus represents abstract, allocentric internal models of the external world at the expense of the fine-grained sensory details present in early visual areas. However, our study joins previous work (Knapen 2021; Silson et al. 2021) in demonstrating that low-level visual coding persists in the hippocampus, and further expands upon that work by characterizing the retinotopic code as bivalent in nature and persistent at rest.

Hippocampal pRFs remain constrained by classic sensory features such as contralateral visual field bias, as in visual (Hemond et al. 2007; Wandell et al. 2007; Chan et al. 2010; Groen et al. 2022a) and higher order cortex (Szinte and Knapen 2020; Knapen 2021; Silson et al. 2021; Steel et al. 2024b). This reinforces the idea that visual field preferences are encoded in higher order, mnemonic cortex. Unlike in perceptual regions — where +pRFs are the majority of retinotopic voxels — the hippocampus contains a balanced mixture of positive and negative retinotopic populations distributed throughout the structure. Rather than reflecting a progressive transformation from purely perceptual to purely mnemonic coding within the hippocampus, this organization indicates that perceptual and mnemonic representations are intermixed within the hippocampus itself. This balanced architecture suggests a close linkage between the hippocampus and vision (Nau et al. 2018; Turk-Browne 2019), while also underscoring the importance of negative retinotopic responses in mnemonic circuitry (Szinte and Knapen 2020; Steel et al. 2024b, 2024a). Together, these findings support the view that specifically bivalent retinotopy is a broader organizational principle in higher-order mnemonic regions, structuring persistent interactions with visual cortex.

Integration with Other Hippocampal Neural Codes

At first glance, the presence of a bivalent retinotopic code in the human hippocampus seems at odds with canonical descriptions of allocentric, spatial selectivity often described in the hippocampus in electrophysiology studies (O'Keefe and Dostrovsky 1971; Moser et al. 2008). However, recent work suggests a complex, multi-faceted view of hippocampal activity that accommodates both response types — particularly when contrasting rodents with non-human primates (Piza et al. 2024). In freely moving macaques and marmosets, canonical place responses rarely exist as pure representations of spatial location (Gulli et al. 2020; Mao et al. 2021; Piza et al. 2024). Instead, hippocampal neurons most commonly present a multiplexed representation of allocentric space along with egocentric features including head direction, facing location, or gaze.

Hippocampal egocentric visual codes are thought to be more prevalent in primates than in rodents due to differences in the spatial exploration strategy between species (Piza et al. 2024). Rodents are nocturnal, and supplement relatively coarse visual information with whisking and

olfaction within their immediate surroundings to build a model of the environment (Piza et al. 2024). In contrast, diurnal primates rely more on long-range visual information, with spatial exploration largely occurring while stationary via head turns and shifts in gaze (Piza et al. 2024). Yet even rodents display significant hippocampal mixed-selectivity to visual information (Acharya et al. 2016), with visual stimulation alone being sufficient to drive a subset of place cells in mice (Chen et al. 2013) and significant overlap (78%) between hippocampal neurons sensitive to egocentric visual stimuli and allocentric position (Purandare et al. 2022).

Within this broader framework of mixed selectivity, the relatively sparse retinotopic code we observe here (~9% of hippocampal voxels) likely co-exists with spatiotopic codes of place and grid cells. Indeed, computational models of hippocampal dynamics suggest that place and grid cells could still serve as the dominant structure for information processing in the hippocampus, providing pre-structured states to support memory encoding in both spatial and non-spatial tasks, with sensory information applied to the scaffold of these pre-structured states, like clothes to a clothesline (Chandra et al. 2025). Future research should explore whether, in humans, the bivalent retinotopic code detected in this study is overlaid on top of place and grid cell representations, or whether it constitutes an independent contributing code that interacts with these spatial representations.

Functional Relevance of Bivalent Hippocampal Retinotopy

Recent work in cortex suggests that bivalent retinotopy at the apex of the cortical hierarchy structures a push-pull dynamic between perceptual and mnemonic systems (Steel et al. 2024b, 2024a). We observe a similar oppositional relationship within the hippocampus itself: pRFs of opposite valence exhibit anti-correlated activity, indicating an intrinsic push–pull architecture. Critically, whereas previous work described this relationship between different, functionally specialized regions (Steel et al. 2024b) and networks (Steel et al. 2024a), the present findings demonstrate this organization within a single mnemonic structure. For example, a recent study found the externally-oriented Dorsal Attention Network and internally-oriented Default Network, classically among the most functionally independent networks, show resting-state interactions structured by retinotopic valence and alignment (Steel et al. 2024a). The hippocampus appears to recapitulate this antagonistic logic at a local scale.

What functional role might such a bivalent code serve? One possibility is that it supports the coordination of perceptual encoding and mnemonic retrieval. In this context, opposing retinotopic populations could provide a spatial mechanism for separating concurrent cognitive operations while preserving a shared visuospatial reference frame, akin to the role of hippocampal theta oscillations in temporally separating encoding and retrieval-related processes (Hasselmo et al. 2002; Kunec et al. 2005; Hasselmo and Stern 2014; Kerrén et al. 2018). Notably, eye-movements provide a compelling link between visual input, the theta rhythm (e.g. eye-movement locked resetting; Hoffman et al. 2013; Jutras et al. 2013; Doucet et al. 2020), and hippocampally-dependent behavior (Wynn et al. 2020a, 2020b; Favila and Aly 2023; Setton et al. 2024). Visual input, via retinotopic coding and theta dynamics, may thus allow the hippocampus to coordinate perceptual and mnemonic functions while maintaining functional separation, ensuring the efficient integration of sensory and mnemonic information.

Alternatively, the bivalent retinotopic code may reflect predictive coding processes (Steel et al. 2024b), thought to be another function of the hippocampus (Wirth 2023). In this framework, negative pRFs could encode top-down sensory predictions, whereas positive pRFs reflect bottom-up sensory drive. Their antagonistic interaction would enable rapid detection of mismatches between expected and observed input, thereby supporting the updating of mnemonic representations. Future work should investigate whether valence-specific populations differentially track prediction errors or encode predictive templates during memory-guided perception.

Open Questions and Future Directions

Several open questions lie beyond the scope of the present study. While we have shown that hippocampal responses during a retinotopic mapping task are robustly fit by a pRF model, this does not verify that these responses are fundamentally retinotopic in nature. Notably, work describing view-selective cells in the primate hippocampus (Rolls and O'Mara 1995; Liu et al. 2017; Corrigan et al. 2023; Piza et al. 2024) suggests an alternative spatiotopic explanation in which hippocampal responses are linked to locations within a visual view, rather than locations of stimulation on the retina. Because participants were instructed to maintain fixation in this study, it was not possible to disentangle spatiotopic and retinotopic representations, and further studies with modified fixation parameters are needed. Similarly, the temporal continuity of the moving bar stimulus makes it difficult to assess what impact, if any, predictive responses may be playing in visually-evoked hippocampal responses.

The present data also leave unresolved questions about temporal dynamics. Although we show reliable spatial segregation of positive and negative retinotopic responses, the temporal resolution of fMRI (here, a 1.33s TR) precludes precise characterization of their timing. As noted above, the hippocampal theta oscillation has also been implicated in sensory-mnemonic processing and integration (Hasselmo et al. 2002; Kunec et al. 2005; Hoffman et al. 2013; Jutras et al. 2013; Hasselmo and Stern 2014; Doucet et al. 2020), and the bivalent retinotopic responses we observe may be shaped by oscillatory dynamics. Further studies exploring hippocampal retinotopic responses with greater temporal resolution, such as with MEG or intracranial recordings, are needed to resolve this interaction and to achieve a level of temporal characterization comparable to that established for early visual retinotopic codes (Yuasa et al. 2023; Groen et al. 2022b).

To summarize, we identified a bivalent retinotopic code in the human hippocampus, which structures voxel-wise interactions within this mnemonic structure. This bivalent retinotopic scaffold may allow for the segregation and integration of perceptual and mnemonic information. By demonstrating that egocentric visual field coding persists within hippocampal circuitry, these findings expand the known extent of retinotopic organization in the human brain and establish a framework for investigating how this code contributes to memory-guided behavior.

References

Acharya L, **Aghajan ZM**, **Vuong C**, **Moore JJ**, **Mehta MR**. Causal Influence of Visual Cues on Hippocampal Directional Selectivity. *Cell* 164: 197–207, 2016.

Alexander AS, **Place R**, **Starrett MJ**, **Chrastil ER**, **Nitz DA**. Rethinking retrosplenial cortex: Perspectives and predictions. *Neuron* 111: 150–175, 2023.

Allen EJ, **St-Yves G**, **Wu Y**, **Breedlove JL**, **Prince JS**, **Dowdle LT**, **Nau M**, **Caron B**, **Pestilli F**, **Charest I**, **Hutchinson JB**, **Naselaris T**, **Kay K**. A massive 7T fMRI dataset to bridge cognitive neuroscience and artificial intelligence. *Nat Neurosci* 25: 116–126, 2022.

Beckers AB, **Drenthen GS**, **Jansen JFA**, **Backes WH**, **Poser BA**, **Keszthelyi D**. Comparing the efficacy of data-driven denoising methods for a multi-echo fMRI acquisition at 7T. *NeuroImage* 280: 120361, 2023.

Beckmann CF, **Smith SM**. Probabilistic independent component analysis for functional magnetic resonance imaging. *IEEE Transactions on Medical Imaging* 23: 137–152, 2004.

Benson NC, **Jamison KW**, **Arcaro MJ**, **Vu AT**, **Glasser MF**, **S. Coalson T**, **Essen DCV**, **Yacoub E**, **Ugurbil K**, **Winawer J**, **Kay K**. The Human Connectome Project 7 Tesla retinotopy dataset: Description and population receptive field analysis. *Journal of Vision* 18: 23–23, 2018.

Chan AW-Y, **Kravitz DJ**, **Truong S**, **Arizpe J**, **Baker CI**. Cortical representations of bodies and faces are strongest in commonly experienced configurations. *Nat Neurosci* 13: 417–418, 2010.

Chandra S, **Sharma S**, **Chaudhuri R**, **Fiete I**. Episodic and associative memory from spatial scaffolds in the hippocampus. *Nature* 1–13, 2025.

Chen G, **King JA**, **Burgess N**, **O'Keefe J**. How vision and movement combine in the hippocampal place code. *Proceedings of the National Academy of Sciences* 110: 378–383, 2013.

Clark BJ, **Simmons CM**, **Berkowitz LE**, **Wilber AA**. The retrosplenial-parietal network and reference frame coordination for spatial navigation. *Behavioral Neuroscience* 132: 416–429, 2018.

Cohen NJ, **Eichenbaum H**. *Memory, Amnesia, and the Hippocampal System*. MIT Press, 1993.

Cohen NJ, **Squire LR**. Preserved Learning and Retention of Pattern-Analyzing Skill in Amnesia: Dissociation of Knowing How and Knowing that. *Science* 210: 207–210, 1980.

Cox RW. AFNI: software for analysis and visualization of functional magnetic resonance neuroimages. *Comput Biomed Res* 29: 162–173, 1996.

Cox RW. AFNI: What a long strange trip it's been. *Neuroimage* 62: 743–747, 2012.

Doucet G, **Gulli RA**, **Corrigan BW**, **Duong LR**, **Martinez-Trujillo JC**. Modulation of local field potentials and neuronal activity in primate hippocampus during saccades. *Hippocampus* 30: 192–209, 2020.

Du J, **DiNicola LM**, **Angeli PA**, **Saadon-Grosman N**, **Sun W**, **Kaiser S**, **Ladopoulou J**, **Xue A**, **Yeo BTT**, **Eldaief MC**, **Buckner RL**. Organization of the human cerebral cortex estimated within individuals: Networks, global topography, and function. *J Neurophysiol* 131: 1014–1082, 2024.

Dumoulin SO, **Wandell BA**. Population receptive field estimates in human visual cortex. *NeuroImage* 39: 647–660, 2008.

Eichenbaum H, **Cohen NJ**. Can We Reconcile the Declarative Memory and Spatial Navigation Views on Hippocampal Function? *Neuron* 83: 764–770, 2014.

Favila SE, **Aly M**. Hippocampal mechanisms resolve competition in memory and perception. *bioRxiv* 2023.10.09.561548, 2023.

Felleman DJ, **Van Essen DC**. Distributed Hierarchical Processing in the Primate Cerebral Cortex. *Cerebral Cortex* 1: 1–47, 1991.

Greicius MD, **Srivastava G**, **Reiss AL**, **Menon V**. Default-mode network activity distinguishes Alzheimer's disease from healthy aging: Evidence from functional MRI. *Proc Natl Acad Sci USA* 101: 4637–4642, 2004.

Griffanti L, **Douaud G**, **Bijsterbosch J**, **Evangelisti S**, **Alfaro-Almagro F**, **Glasser MF**, **Duff EP**, **Fitzgibbon S**, **Westphal R**, **Carone D**, **Beckmann CF**, **Smith SM**. Hand classification of fMRI ICA noise components. *NeuroImage* 154: 188–205, 2017.

Griffanti L, **Salimi-Khorshidi G**, **Beckmann CF**, **Auerbach EJ**, **Douaud G**, **Sexton CE**, **Zsoldos E**, **Ebmeier KP**, **Filippini N**, **Mackay CE**, **Moeller S**, **Xu J**, **Yacoub E**, **Baselli G**, **Ugurbil K**, **Miller KL**, **Smith SM**. ICA-based artefact removal and accelerated fMRI acquisition for improved resting state network imaging. *NeuroImage* 95: 232–247, 2014.

Groen IIA, **Dekker TM**, **Knapen T**, **Silson EH**. Visuospatial coding as ubiquitous scaffolding for human cognition. *Trends in Cognitive Sciences* 26: 81–96, 2022a.

Groen IIA, **Piantoni G**, **Montenegro S**, **Flinker A**, **Devore S**, **Devinsky O**, **Doyle W**, **Dugan P**, **Friedman D**, **Ramsey NF**, **Petridou N**, **Winawer J**. Temporal Dynamics of Neural Responses in Human Visual Cortex. *J Neurosci* 42: 7562–7580, 2022b.

Gulli RA, **Duong LR**, **Corrigan BW**, **Doucet G**, **Williams S**, **Fusi S**, **Martinez-Trujillo JC**. Context-dependent representations of objects and space in the primate hippocampus during virtual navigation. *Nat Neurosci* 23: 103–112, 2020.

Hasselmo ME, **Bodelón C**, **Wyble BP**. A Proposed Function for Hippocampal Theta Rhythm: Separate Phases of Encoding and Retrieval Enhance Reversal of Prior Learning. *Neural Computation* 14: 793–817, 2002.

Hasselmo ME, **Stern CE**. Theta rhythm and the encoding and retrieval of space and time. *NeuroImage* 85: 656–666, 2014.

Hemond CC, **Kanwisher NG**, **Beeck HPO de**. A Preference for Contralateral Stimuli in Human Object- and Face-Selective Cortex. *PLOS ONE* 2: e574, 2007.

Hoffman KL, **Dragan MC**, **Leonard TK**, **Micheli C**, **Montefusco-Siegmund R**, **Valiante TA**. Saccades during visual exploration align hippocampal 3–8 Hz rhythms in human and non-human primates. *Front Syst Neurosci* 7, 2013.

Jeffery KJ. Integration of the sensory inputs to place cells: What, where, why, and how? *Hippocampus* 17: 775–785, 2007.

Jutras MJ, **Fries P**, **Buffalo EA**. Oscillatory activity in the monkey hippocampus during visual exploration and memory formation. *Proceedings of the National Academy of Sciences* 110: 13144–13149, 2013.

Kahn I, **Andrews-Hanna JR**, **Vincent JL**, **Snyder AZ**, **Buckner RL**. Distinct cortical anatomy linked to subregions of the medial temporal lobe revealed by intrinsic functional connectivity. *J Neurophysiol* 100: 129–139, 2008.

Kerrén C, **Linde-Domingo J**, **Hanslmayr S**, **Wimber M**. An Optimal Oscillatory Phase for Pattern Reactivation during Memory Retrieval. *Current Biology* 28: 3383-3392.e6, 2018.

Klink PC, **Chen X**, **Vanduffel W**, **Roelfsema PR**. Population receptive fields in nonhuman primates from whole-brain fMRI and large-scale neurophysiology in visual cortex. *eLife* 10: e67304, 2021.

Knapen T. Topographic connectivity reveals task-dependent retinotopic processing throughout the human brain. *Proceedings of the National Academy of Sciences* 118: e2017032118, 2021.

Kunec S, **Hasselmo ME**, **Kopell N**. Encoding and Retrieval in the CA3 Region of the Hippocampus: A Model of Theta-Phase Separation. *Journal of Neurophysiology* 94: 70–82, 2005.

Mao D, **Avila E**, **Caziot B**, **Laurens J**, **Dickman JD**, **Angelaki DE**. Spatial modulation of hippocampal activity in freely moving macaques. *Neuron* 109: 3521-3534.e6, 2021.

Moser EI, **Kropff E**, **Moser M-B**. Place Cells, Grid Cells, and the Brain's Spatial Representation System. *Annual Review of Neuroscience* 31: 69–89, 2008.

Nau M, **Julian JB**, **Doeller CF**. How the Brain's Navigation System Shapes Our Visual Experience. *Trends in Cognitive Sciences* 22: 810–825, 2018.

O'Keefe J, **Dostrovsky J**. The hippocampus as a spatial map. Preliminary evidence from unit activity in the freely-moving rat. *Brain Res* 34: 171–175, 1971.

Pereira A, **Ribeiro S**, **Wiest M**, **Moore LC**, **Pantoja J**, **Lin S-C**, **Nicolelis MAL**. Processing of tactile information by the hippocampus. *Proceedings of the National Academy of Sciences* 104: 18286–18291, 2007.

Piza DB, **Corrigan BW**, **Gulli RA**, **Do Carmo S**, **Cuello AC**, **Muller L**, **Martinez-Trujillo J**. Primacy of vision shapes behavioral strategies and neural substrates of spatial navigation in marmoset hippocampus. *Nat Commun* 15: 4053, 2024.

Poppenk J, **Evensmoen HR**, **Moscovitch M**, **Nadel L**. Long-axis specialization of the human hippocampus. *Trends Cogn Sci* 17: 230–240, 2013.

Purandare CS, **Dhingra S**, **Rios R**, **Vuong C**, **To T**, **Hachisuka A**, **Choudhary K**, **Mehta MR**. Moving bar of light evokes vectorial spatial selectivity in the immobile rat hippocampus. *Nature* 602: 461–467, 2022.

Rolls ET. A Theory and Model of Scene Representations With Hippocampal Spatial View Cells. *Hippocampus* 35: e70013, 2025.

Saad ZS, **Gotts SJ**, **Murphy K**, **Chen G**, **Jo HJ**, **Martin A**, **Cox RW**. Trouble at Rest: How Correlation Patterns and Group Differences Become Distorted After Global Signal Regression. *Brain Connectivity* 2: 25–32, 2012.

Scoville WB, **Milner B**. Loss of recent memory after bilateral hippocampal lesions. *J Neurol Neurosurg Psychiatry* 20: 11–21, 1957.

Sereno MI, **Allman JM**. Cortical Visual Areas in Mammals [Online]. In: *The Neural Basis of Visual Function*. Macmillan, p. 160–172.https://pages.ucsd.edu/~msereno/papers/VisualAreas91.pdf [4 May 2025].

Setton R, **Wynn JS**, **Schacter DL**. Peering into the future: Eye movements predict neural repetition effects during episodic simulation. *Neuropsychologia* 197: 108852, 2024.

Silson EH, **Chan AW-Y**, **Reynolds RC**, **Kravitz DJ**, **Baker CI**. A Retinotopic Basis for the Division of High-Level Scene Processing between Lateral and Ventral Human Occipitotemporal Cortex. *J Neurosci* 35: 11921–11935, 2015.

Silson EH, **Zeidman P**, **Knapen T**, **Baker CI**. Representation of Contralateral Visual Space in the Human Hippocampus. *J Neurosci* 41: 2382–2392, 2021.

Steel A, **Angeli PA**, **Silson EH**, **Robertson CE**. Retinotopic coding organizes the interaction between internally and externally oriented brain networks. bioRxiv: 2024.09.25.615084, 2024a.

Steel A, **Billings MM**, **Silson EH**, **Robertson CE**. A network linking scene perception and spatial memory systems in posterior cerebral cortex. *Nat Commun* 12: 2632, 2021a.

Steel A, **Garcia BD**, **Goyal K**, **Mynick A**, **Robertson CE**. Scene Perception and Visuospatial Memory Converge at the Anterior Edge of Visually Responsive Cortex. *J Neurosci* 43: 5723–5737, 2023.

Steel A, **Garcia BD**, **Prasad D**, **Robertson CE**. Relating scene memory and perception activity to functional properties, networks, and landmarks of posterior cerebral cortex – A probabilistic atlas. bioRxiv: 2025.01.06.631538, 2025.

Steel A, **Robertson CE**, **Taube JS**. Current Promises and Limitations of Combined Virtual Reality and Functional Magnetic Resonance Imaging Research in Humans: A Commentary on Huffman and Ekstrom (2019). *Journal of Cognitive Neuroscience* 33: 159–166, 2021b.

Steel A, **Silson EH**, **Garcia BD**, **Robertson CE**. A retinotopic code structures the interaction between perception and memory systems. *Nat Neurosci* 27: 339–347, 2024b.

Strange BA, **Witter MP**, **Lein ES**, **Moser EI**. Functional organization of the hippocampal longitudinal axis. *Nat Rev Neurosci* 15: 655–669, 2014.

Szinte M, **Knapen T**. Visual Organization of the Default Network. *Cerebral Cortex* 30: 3518–3527, 2020.

Taylor PA, **Glen DR**, **Chen G**, **Cox RW**, **Hanayik T**, **Rorden C**, **Nielson DM**, **Rajendra JK**, **Reynolds RC**. A Set of FMRI Quality Control Tools in AFNI: Systematic, in-depth and interactive QC with afni_proc.py and more. *bioRxiv* 2024.03.27.586976, 2024.

Tootell RBH, **Hadjikhani NK**, **Mendola JD**, **Marrett S**, **Dale AM**. From retinotopy to recognition: fMRI in human visual cortex. *Trends in Cognitive Sciences* 2: 174–183, 1998.

Turk-Browne NB. The hippocampus as a visual area organized by space and time: A spatiotemporal similarity hypothesis. *Vision Research* 165: 123–130, 2019.

Vann SD, **Aggleton JP**, **Maguire EA**. What does the retrosplenial cortex do? *Nat Rev Neurosci* 10: 792–802, 2009.

Vincent JL, **Snyder AZ**, **Fox MD**, **Shannon BJ**, **Andrews JR**, **Raichle ME**, **Buckner RL**. Coherent spontaneous activity identifies a hippocampal-parietal memory network. *J Neurophysiol* 96: 3517–3531, 2006.

Vinogradova O s. Hippocampus as comparator: Role of the two input and two output systems of the hippocampus in selection and registration of information. *Hippocampus* 11: 578–598, 2001.

Wandell BA, **Dumoulin SO**, **Brewer AA**. Visual Field Maps in Human Cortex. *Neuron* 56: 366–383, 2007.

Whitlock JR, **Sutherland RJ**, **Witter MP**, **Moser M-B**, **Moser EI**. Navigating from hippocampus to parietal cortex. *Proceedings of the National Academy of Sciences* 105: 14755–14762, 2008.

Whittington JCR, **Muller TH**, **Mark S**, **Chen G**, **Barry C**, **Burgess N**, **Behrens TEJ**. The Tolman-Eichenbaum Machine: Unifying Space and Relational Memory through Generalization in the Hippocampal Formation. *Cell* 183: 1249-1263.e23, 2020.

Wirth S. A place with a view: A first-person perspective in the hippocampal memory space. *Hippocampus* 33: 658–666, 2023.

Wynn JS, **Amer T**, **Schacter DL**. How Older Adults Remember the World Depends On How They See It. *Trends in Cognitive Sciences* 24: 858–861, 2020a.

Wynn JS, **Ryan JD**, **Buchsbaum BR**. Eye movements support behavioral pattern completion. *Proceedings of the National Academy of Sciences* 117: 6246–6254, 2020b.

Yuasa K, **Groen IIA**, **Piantoni G**, **Montenegro S**, **Flinker A**, **Devore S**, **Devinsky O**, **Doyle W**, **Dugan P**, **Friedman D**, **Ramsey N**, **Petridou N**, **Winawer J**. Precise Spatial Tuning of Visually Driven Alpha Oscillations in Human Visual Cortex. *eLife* 12, 2023.

Supplemental Materials

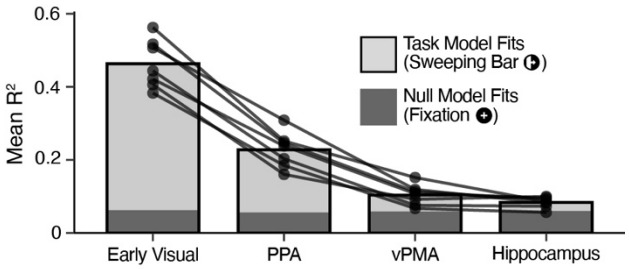

Supplemental Fig 1. *Moving along the visual hierarchy reduces the average model fit, but does not influence the noise floor derived from resting-state fixation. Mixed effects modeling shows that region, rather than mean R^2 value, is the primary driver of -pRF proportion (region: $F(3, 18.308) = 9.712$, $p < 0.001$; mean R^2: $F(1, 22.996) = 0.185$, $p = 0.672$).*